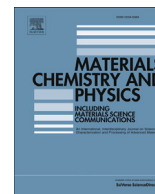




Contents lists available at ScienceDirect

Materials Chemistry and Physics

journal homepage: www.elsevier.com/locate/matchemphys

Influence of structure of $\text{Fe}_2\text{O}_3\text{--In}_2\text{O}_3$ nanocomposites on the sensitivity of thin-film sensors on their base

Dzmitry Kotsikau ^{a, *}, Maria Ivanovskaya ^b^a Belarusian State University, 14 Leningradskaya, 220030 Minsk, Belarus^b Research Institute for Physical-Chemical Problems of the Belarusian State University, 14 Leningradskaya, 220030 Minsk, Belarus

HIGHLIGHTS

- Gas-sensing $\text{Fe}_2\text{O}_3\text{--In}_2\text{O}_3$ composites were prepared by inorganic sol–gel approach.
- Structure of $\text{Fe}_2\text{O}_3\text{--In}_2\text{O}_3$ composites are strongly dependent on synthesis conditions.
- Sensitivity of $\text{Fe}_2\text{O}_3\text{--In}_2\text{O}_3$ thin films were correlated with their structural features.
- Condition optimal for the detection of NO_2 , O_3 and $\text{C}_2\text{H}_5\text{OH}$ has been revealed.
- Thin films based on $\gamma\text{-Fe}_2\text{O}_3$ phase demonstrate a high response to NO_2 .

ARTICLE INFO

Article history:

Received 8 October 2014

Received in revised form

14 March 2015

Accepted 25 April 2015

Available online xxx

Keywords:

Oxides

Sol–gel growth

Microstructure

Semiconductivity

Nanostructures

Electrical properties

ABSTRACT

Thin-film sensing layers based on $\text{Fe}_2\text{O}_3\text{--In}_2\text{O}_3$ nanocomposites with different component ratio and structural features were synthesized by inorganic modification of sol–gel method. The phase composition and morphology of the composites as a function of the synthesis conditions were studied by X-ray diffraction, transmission electron microscopy, electron diffraction, differential scanning calorimetry, electron paramagnetic resonance and infrared spectroscopy. The gas-sensing parameters the $\text{Fe}_2\text{O}_3\text{--In}_2\text{O}_3$ composites were correlated with their structure. The synthesis conditions resulting in the formation in the $\text{Fe}_2\text{O}_3\text{--In}_2\text{O}_3$ composites of metastable $\gamma\text{-Fe}_2\text{O}_3$ phase, which is characterized by an enhanced activity in adsorption and catalysis as compared to $\alpha\text{-Fe}_2\text{O}_3$ oxide, were revealed. An improved sensitivity of $\gamma\text{-Fe}_2\text{O}_3$ based composites to different gases was shown. The chemical and structural compositions of $\text{Fe}_2\text{O}_3\text{--In}_2\text{O}_3$ thin-film sensing layers and operating temperatures optimal for the detection of O_3 , NO_2 and $\text{C}_2\text{H}_5\text{OH}$ were proposed.

© 2015 Elsevier B.V. All rights reserved.

1. Introduction

Materials based on $\text{Fe}_2\text{O}_3\text{--In}_2\text{O}_3$ mixed oxides in a form of films, powders, ceramics and $\text{In}_2\text{O}_3/\text{Fe}_2\text{O}_3/\text{In}_2\text{O}_3$ multi-layers are considered to be very promising candidates for gas sensors, optoelectronics and spintronics [1–9]. Most of the reported studies of the $\text{Fe}_2\text{O}_3\text{--In}_2\text{O}_3$ system for gas-sensing applications deal with the composite materials in which iron oxide has a phase structure of $\alpha\text{-Fe}_2\text{O}_3$ [4,5,7,8,10]. Due to recent advances in spintronics, materials representing magnetic clusters incorporated into a semiconducting matrix is of great interest [6]. For example, a ferromagnetic

behavior of Fe^{3+} -doped In_2O_3 oxide were studied over the past five years [3,6,9,11]. In these mixed materials, In_2O_3 oxide is a pre-dominating phase while $\alpha\text{-Fe}_2\text{O}_3$ oxide is a magnetic dopant. Depending on the component ratio and the synthesis conditions, the $\text{Fe}_2\text{O}_3\text{--In}_2\text{O}_3$ composites could consist of either two phases ($C\text{-In}_2\text{O}_3$ and $\alpha\text{-Fe}_2\text{O}_3$) or single $C\text{-In}_{2-x}\text{Fe}_x\text{O}_3$ phase, which is a substitutional solid solution with $x \leq 0.4$ [11]. A high mutual solubility of $\alpha\text{-Fe}_2\text{O}_3$ and $C\text{-In}_2\text{O}_3$ oxides was achieved by thermal treatment of co-precipitated hydroxides of Fe^{3+} and In^{3+} [12] or by mechanical activation of the corresponding oxides [13,14]. However, there is a lack of information on the stability of the solid solutions formed.

In contrast, the properties of $\text{Fe}_2\text{O}_3\text{--In}_2\text{O}_3$ composites with a high content of Fe_2O_3 are poorly studied [15,16]. Materials based on $\alpha\text{-Fe}_2\text{O}_3$ oxide doped with single- and double-charged metal cations were characterized in [17,18] as humidity sensors. The

* Corresponding author.

E-mail addresses: kotsikau@bsu.by (D. Kotsikau), ivanovskaya@bsu.by (M. Ivanovskaya).

formation of a ferrite structure is possible in such composites. There are contradictory data about the formation and stabilization of chemical compounds of α -Fe₂O₃ with triple-charged metal cations including In³⁺ [19]. There are no strict evidences whether In₂Fe₄O₉, InFe₂O₄ and InFeO₃ composites are individual compounds or solid solutions based on metastable phases of indium oxides like monoclinic *M*-In₂O₃ and rhombohedral *R*-In₂O₃ [19–21]. It was shown in [22] that the presence of Fe³⁺ ions in indium oxide promotes the formation of *R*-In₂O₃ at low temperature. The emergence of this phase is unwanted for gas-sensing applications due to its lower conductivity and adsorption activity as compared to *C*-In₂O₃.

There is little literature on Fe₂O₃–In₂O₃ composites containing γ -Fe₂O₃ structural modification of iron oxide, which is thermodynamically unstable at temperatures below ~900 °C [1,2,15]. However, γ -Fe₂O₃ phase was reported to be a promising material for gas sensors [1,23,24]. A high sensitivity of thin films of γ -Fe₂O₃ and bilayer films of γ -Fe₂O₃/In₂O₃ to ozone was shown in [1,15,24]. The little interest in γ -Fe₂O₃ based materials is possibly caused by a low stability of both γ -Fe₂O₃ phase and Fe²⁺ compounds, which are frequent precursors or intermediates for the preparation of γ -Fe₂O₃ oxide. During the synthesis, the Fe²⁺ → Fe³⁺ oxidation process should be strictly controlled to obtain the required γ -Fe₂O₃ structure. Otherwise, thermodynamically stable α -Fe₂O₃ phase will be generated [25–27]. Two-component oxides like Fe₂O₃–In₂O₃ are more sensitive to the preparation conditions where minor deviations from the synthesis procedure might cause a strong effect on the structure and properties of the resulting material. The results reported by different authors cannot be always compared properly in order to reveal any regularities and dependences.

The present paper deals with a complex study of the structure and the gas-sensing properties of γ -Fe₂O₃–In₂O₃ and α -Fe₂O₃–In₂O₃ thin-films with the scantily studied compositions (Fe:In = 1:1, 9:1 molar ratios). It was a goal to obtain materials containing either γ -Fe₂O₃ or α -Fe₂O₃ phase modifications, and to prevent the formation of *R*-In₂O₃ phase. The aim of the work was to reveal the effect of chemical composition and synthesis conditions on the phase structure, grain size and gas-sensing features of the Fe₂O₃–In₂O₃ composites prepared by the same method.

2. Material and methods

2.1. Synthesis of oxide composites

The composites were prepared by a modified sol–gel method based on applying aqueous solutions of inorganic precursors [28,29]. This approach allows preparing nanosized metal oxides in forms of colloidal solutions, thin films and powders. The crystallization of the sol–gel derived materials occurs typically at comparatively low temperatures (300–400 °C) suitable for the stabilization of iron oxide in both α -Fe₂O₃ and γ -Fe₂O₃ modifications. The main advantage of the approach used in the study is in the formation of the primary structure of oxide composites at room temperature at the stage of the preparation of the corresponding colloidal solutions, and at the stage of their transformation into gel and xerogel states [30]. This allowed us to control reliably the formation of γ -Fe₂O₃ oxide, which is metastable at low temperatures, and to avoid its transformation into α -Fe₂O₃ modification.

Two series of the In₂O₃–Fe₂O₃ composites were prepared. Series *I* was prepared by a combined hydrolysis of iron and indium salts with ammonia solution as a base agent, and further transformation of the precipitates into a sol state. Series *II* was prepared by a separate hydrolysis of indium or iron salts, and a stabilization of individual indium or iron hydroxides/oxides in a sol state. Then the individual sols were mixed together in the required proportions. The two procedures were applied since the mutual influence of

indium and iron hydroxides on the structure of the resulting product is more pronounced in the case of the combined precipitation technique rather than under the mixing of the separately prepared hydroxides.

Thermally stimulated transformations of the co-precipitated hydroxides (samples of series *I*) are hardly predictable, which can lead to a product with unexpected structural features [31]. In order to ensure a homogeneous and nanosized structure of the resulting composite, a reverse order of the precipitation was used. The reverse order means that solutions of metal salts are to be added to an aqueous ammonia solution taken in some excess to maintain a constant *pH* value (~11) of the reaction mixture over the whole duration of the synthesis [31–33]. Under the given experimental conditions, the hydrolysis of all the salts occurs simultaneously, which is especially critical in the case of combined precipitation of Fe(OH)₂, In(OH)₃ and Fe(OH)₃ hydroxides. The high *pH* value (>10) prevents the generation of the undesired *R*-In₂O₃ structure under subsequent thermal treatment of the oxide composite.

To prepare γ -Fe₂O₃–In₂O₃ and α -Fe₂O₃–In₂O₃ composites containing γ -Fe₂O₃ and α -Fe₂O₃ phases respectively, a number of regularities were taken into account. Namely, the crystallization of In₂O₃ oxide from a sol–gel derived In(OH)₃ hydroxide occurs at 200 °C [31]. The base hydrolysis of Fe³⁺ salts results in amorphous iron hydroxide [25–27,32,33], which transforms into α -Fe₂O₃ oxide at temperatures higher than 300 °C. Two general approaches to the synthesis of γ -Fe₂O₃ oxide were exploited: i) a base hydrolysis of Fe²⁺ salts with the formation of Fe(OH)₂ hydroxide, and its further oxidation with a stream of air or oxygen passed through the suspension at 100 °C [34]; ii) a combined base hydrolysis of Fe³⁺ and Fe²⁺ salts giving FeO·Fe₂O₃ intermediate, and its oxidation as described above [35]. The later approach results typically in smaller γ -Fe₂O₃ particles (~10 nm) with a high content of residual OH-groups as compared to the product of Fe(OH)₂ oxidation whose grain size is about 40 nm. It worth notice that in composite oxide materials, the thermally stimulated crystallization processes of oxide phases proceed normally under the conditions different from those revealed for individual hydroxides [22,30,31,36,37].

2.2. Structural characterization

The phase composition of the samples was characterized by X-ray diffraction (XRD) analysis. Fine structural features of the Fe₂O₃–In₂O₃ composites, which are typically nanosized and poorly crystallized, were revealed by high-resolution transmission electron microscopy (TEM), electron diffraction (ED), differential scanning calorimetry (DSC), infrared spectroscopy (IR), and electron paramagnetic resonance spectroscopy (EPR). The XRD analysis was carried out on a HZG-4A diffractometer by using CoK α radiation. The TEM/ED examinations were performed with a LEO 906E and a JEOL 4000 EX high-resolution transmission electron microscopes. The DSC analysis was performed on a NETCH STA 449 C instrument. The IR analysis of powdered samples was carried out on an AVATAR FTIR-330 spectrometer supplied with a smart diffuse reflectance accessory. The EPR spectra were recorded on a VARIAN spectrometer with resonance frequency of 9.35 GHz (X-band), magnetic field modulation of 25 kHz, modulation amplitude of 1–4 G, and microwave power of 5 mW.

2.3. Fabrication and testing of sensors

In order to obtain thin-film sensors, the prepared sols of the Fe₂O₃–In₂O₃ composites were deposited by spin-coating onto polycrystalline Al₂O₃ substrates (3 × 3 × 0.25 mm³) supplied with Pt interdigitated electrode structure on the front side and Pt-heater on the rear side. The thickness of the thin films was estimated by

SEM analysis to be about 200 nm. The sensor elements were annealed at 400 °C for 96 h in air. The gas-sensing features of the films to C₂H₅OH (50 and 100 ppm), NO₂ and O₃ (0.1 and 0.2 ppm) gases were tested on an 8-channel gas-mixing station with electronic gas flow controllers supplied with a Keithley 2000 multimeter and a computer. A contact electric potential was applied to the interdigitated electrode structure and the current through sensing layers was measured in air (I_{air}) and in air-gas mixtures (I_{gas}). The response (S) of the sensors was calculated as $I_{\text{air}}/I_{\text{gas}}$ or as $I_{\text{gas}}/I_{\text{air}}$ when detecting oxidizing (NO₂, O₃) and reducing (C₂H₅OH) gases, respectively. The time that it takes the sensor to be within 10% of the response value it had before the exposure to a gas was taken as the recovery time (t_{rec}). The measurements were carried out in a flow chamber (0.2 l) at 0.3 l min⁻¹ flow rate, 20 °C temperature and 30% relative humidity (RH). Since the conductivity of the sensing layers under study is a complex function of their chemical composition, phase structure, grain size and operating temperature, all the measurement were limited to a fixed humidity level. The detailed results on the influence of humidity on the electric conductivity of thin-film layers based on oxide composites are given elsewhere [17,18].

The required concentrations of NO₂ and C₂H₅OH gases were obtained by diluting certified gas mixtures with synthetic air on the gas-mixing station controlled by a computer. Ozone was generated by exposure air to ultra-violet radiation. Its concentrations were acquired by an electrochemical technique.

3. Results and discussions

3.1. Structural characterization of the composites

The phase composition and the grain size of the studied Fe₂O₃–In₂O₃ samples annealed at 400 °C are summarized in Table 1 as a function of the synthesis conditions. The XRD patterns of the Fe₂O₃–In₂O₃ (9:1) composites prepared via different precursors and annealed at 300–800 °C are given in Fig. 1.

One can indicate certain regularities of the structure formation in the Fe₂O₃–In₂O₃ composites prepared via the inorganic sol–gel

route. All the synthesized samples are nano-scaled with the grain size ranging from 2 to 30 nm. There is a clear mutual influence of the components on the formation of the binary composite structure under thermal treatment of the corresponding sols and xerogels (dried gels). An inhibition of the crystallization processes of oxide phases and smaller grain size are typical of the composites as compared to individual iron and indium oxides. According to the ED analysis, the hydrolysis of Fe³⁺ salts (samples 1, 11, 12) always results in α -Fe₂O₃ structure after thermal treatment of the powders at 300 °C (see Table 1). These samples being heated at temperatures less than 400 °C remain nanosized and X-ray amorphous. The XRD analysis allows registering α -Fe₂O₃ phase in the powders annealed at 500 °C. A mutual doping of α -Fe₂O₃ and C-In₂O₃ oxides was found to take place resulting in substitutional solid solutions. This conclusion follows from the analysis of the lattice constants acquired by the XRD technique for the Fe₂O₃–In₂O₃ composites with different component ratios. Thus, the increased constants of α -Fe₂O₃ phase doped with indium ions (Fe_{2-x}In_xO₃ solid solution, e.g. sample 11, $a = 0.505$ nm, $c = 1.379$ nm), and the decreased constant of C-In₂O₃ phase doped with iron ions (In_{2-x}Fe_xO₃ solid solution, e.g. sample 12, $a = 1.005$ nm) as compared to the data for pure α -Fe₂O₃ ($a = 0.504$ nm, $c = 1.375$ nm) and C-In₂O₃ ($a = 1.012$ nm) oxides were observed.

At Fe:In = 1:1 molar ratio, the major phase occurred in the Fe₂O₃–In₂O₃ nanocomposites is cubic indium oxide (C-In₂O₃) with the a lattice constant decreased comparing to the pure indium oxide (samples 2, 4, 6, 8, 10, 12). In the mentioned samples, α -Fe₂O₃ phase is X-ray amorphous but it was registered by the ED method. The formation of metastable indium oxide phases like M-In₂O₃ and R-In₂O₃ or indium ferrite phases was not revealed by using the diffraction techniques.

The combined hydrolysis of Fe²⁺ and In³⁺ salts does not lead to the formation of γ -Fe₂O₃ structure. A thermal treatment of the coprecipitated In(OH)₃ and Fe(OH)₂ hydroxides results in α -Fe₂O₃ oxide. Under the given synthesis conditions, the presence of In³⁺ ions inhibits the crystallization of γ -Fe₂O₃ phase. In contrast, the stabilization of γ -Fe₂O₃ structure is observed under heating the mixtures of the separately prepared hydroxides: Fe(OH)₂ + In(OH)₃ or Fe₃O₄· n H₂O + In(OH)₃ (samples 7–10). The γ -Fe₂O₃ → α -Fe₂O₃ phase transition registered for the mixed composites by DSC technique shifts towards higher temperatures (485–500 °C) as compared to pure γ -Fe₂O₃ oxide (~450 °C). The γ -Fe₂O₃ is the predominant phase in samples 7 and 9, which have Fe:In = 9:1 ratio. According to the Mössbauer spectroscopy studies undertaken in [1,15], the solubility of In³⁺ ions in spinel-type γ -Fe₂O₃ with the formation of solid solution is lower than in α -Fe₂O₃ phase.

Sample 5 synthesized by the combined hydrolysis of Fe³⁺, Fe²⁺ and In³⁺ salts is characterized by a complex structure and morphology. According to the TEM and ED data, the composite consists of three phases – anisotropic particles with tetragonal Q- γ -Fe₂O₃ lattice (JCPDS 25-1402), spherical particles with cubic C- γ -Fe₂O₃ lattice (JCPDS 39-1346), and spherical particles of rhombohedral α -Fe₂O₃ phase (JCPDS 33-0664) doped with In³⁺ ions (In³⁺– α -Fe₂O₃ substitutional solid solution).

The IR spectra given in Fig. 2 also indicate the formation of Q- γ -Fe₂O₃ phase in sample 5. The Q- γ -Fe₂O₃ and C- γ -Fe₂O₃ structures can be distinguished using IR-spectroscopy by the position of an absorption band attributed to ν (Fe–O) vibration, which is the most sensitive to [FeO₄]:[FeO₆] ratio [38]. The maximum intensity of ν (Fe–O) band in the IR spectrum of sample 5 was registered at 548 cm⁻¹ this value corresponds to the [FeO₄]:[FeO₆] ratio typical of Q- γ -Fe₂O₃ structure. In the spectra of the samples 7 and 9 containing C- γ -Fe₂O₃ phase, the mentioned absorption band was found at 560–570 cm⁻¹. The anisotropy of the obtained Q- γ -Fe₂O₃

Table 1

The structural features of the Fe₂O₃–In₂O₃ composites annealed at 400 °C

No	Precursors	Fe:In mol. ratio	Phase composition ^a	Grain size, nm
<i>Series I (combined hydrolysis)</i>				
1	Fe ³⁺ , In ³⁺	9:1	α -Fe ₂ O ₃	2–4
2		1:1	C-In ₂ O ₃	5–8
3	Fe ²⁺ , In ³⁺	9:1	α -Fe ₂ O ₃	3–6
4		1:1	C-In ₂ O ₃	5–8
			α -Fe ₂ O ₃	5–6
5	Fe ²⁺ , Fe ³⁺ , In ³⁺	9:1	Q- γ -Fe ₂ O ₃	10 × 30
			C- γ -Fe ₂ O ₃	2–4
			α -Fe ₂ O ₃	2–4
6		1:1	C-In ₂ O ₃	5–8
			α -Fe ₂ O ₃	
<i>Series II (mixing separately prepared sols)</i>				
7	In(OH) ₃ , Fe ₃ O ₄	9:1	C- γ -Fe ₂ O ₃	4–5
			C-In ₂ O ₃	5–8
8		1:1	C-In ₂ O ₃	7–8
			C- γ -Fe ₂ O ₃	5–6
9	In(OH) ₃ , Fe(OH) ₂	9:1	C- γ -Fe ₂ O ₃	8–10
			C-In ₂ O ₃	5–6
10		1:1	C-In ₂ O ₃	7–8
			C- γ -Fe ₂ O ₃	
11	In(OH) ₃ , Fe(OH) ₃	9:1	α -Fe ₂ O ₃	3–8
12		1:1	C-In ₂ O ₃	5–8
			α -Fe ₂ O ₃	3–6

^a The phases denoted here as α -Fe₂O₃ and C-In₂O₃ are actually substitutional solid solutions α -Fe_{2-x}In_xO₃ and C-In_{2-x}Fe_xO₃, respectively.

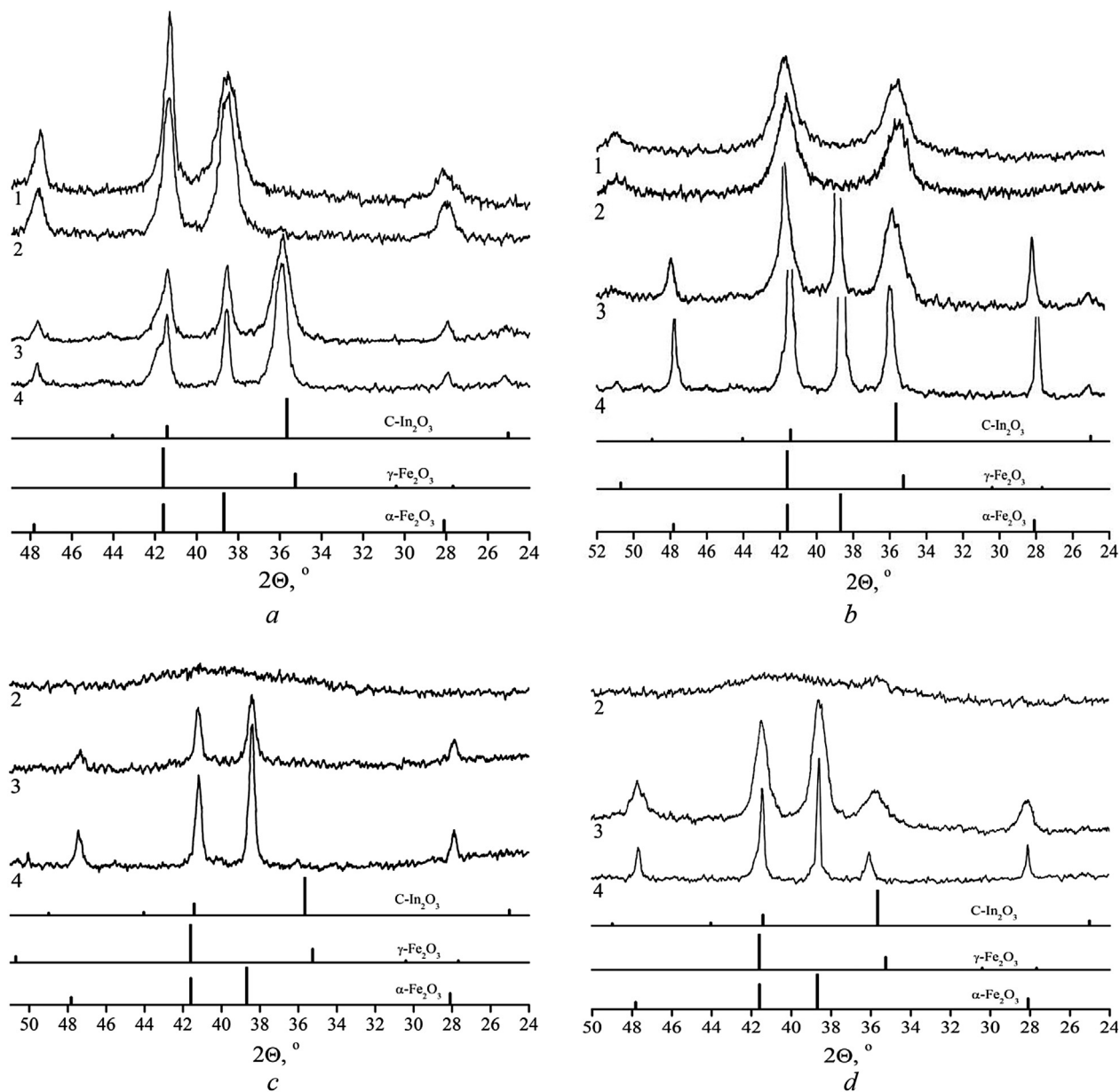


Fig. 1. The XRD patterns of the $\text{Fe}_2\text{O}_3\text{-In}_2\text{O}_3$ (9:1) composites prepared by different routes as a function of the annealing temperature (1–300 °C; 2–400 °C; 3–500 °C; 4–800 °C): a – sample 5; b – sample 7; c – sample 1; d – sample 11.

grains is evoked by the ordering of cation vacancies [39]. As a rule, a highly dispersed $C\text{-}\gamma\text{-Fe}_2\text{O}_3$ phase with Fe^{3+} cations randomly distributed over the tetra- and octahedral positions of the spinel crystal lattice forms at low temperature [25,40]. The stabilization of the tetragonal structure is not typical at low temperatures. Needle-shape $Q\text{-}\gamma\text{-Fe}_2\text{O}_3$ particles with the ordered distribution of Fe^{3+} ions and the cation vacancies might be prepared by a high-temperature decomposition of $\alpha\text{-FeOOH}$ powder [41]. The formation of $Q\text{-}\gamma\text{-Fe}_2\text{O}_3$ phase in sample 5 at low temperature can be caused by the effect of In^{3+} ions on the crystallization of iron oxide starting from the product of the combined hydrolysis of Fe^{2+} , Fe^{3+} and In^{3+} salts. There is literature reporting the formation of $Q\text{-}\gamma\text{-Fe}_2\text{O}_3$ phase at low temperature in the presence of some modifiers like Sn^{4+} ions [42], and a partial reduction of iron oxide to $\text{Fe}_2\text{O}_{2.97}$ composition [43].

It follows from the XRD data that the phase composition of the samples under study remains unchanged within the annealing

temperature range of 300–400 °C. As determined by DSC-TG and XRD methods, noticeable structural transformations proceed in the samples at temperatures higher than 450 °C.

First, the $\gamma\text{-Fe}_2\text{O}_3 \rightarrow \alpha\text{-Fe}_2\text{O}_3$ phase transition occurs at 455–550 °C depending on the sample composition. Then, both $\text{Fe}_{2-x}\text{In}_x\text{O}_3$ and $\text{In}_{2-x}\text{Fe}_x\text{O}_3$ solid solutions decompose to give separate iron oxide and indium oxide phases. In the most thermally stable composites, the phase separation occurs at 800 °C. Note that all the $\text{Fe}_2\text{O}_3\text{-In}_2\text{O}_3$ samples studied here being annealed at 800 °C consist of $\alpha\text{-Fe}_2\text{O}_3$ and $C\text{-In}_2\text{O}_3$ oxides. Therefore, a thermal treatment of the $\text{Fe}_2\text{O}_3\text{-In}_2\text{O}_3$ sensing layers at 400 °C for 96 h is expected to be sufficient to ensure the stability of their phase composition and morphology at the sensor operation temperatures used in this study (≤ 300 °C). The gas-sensing features were proved to be stable during a long-term operation of the sensors. This confirms indirectly the assumption that their structural features remain unchanged.

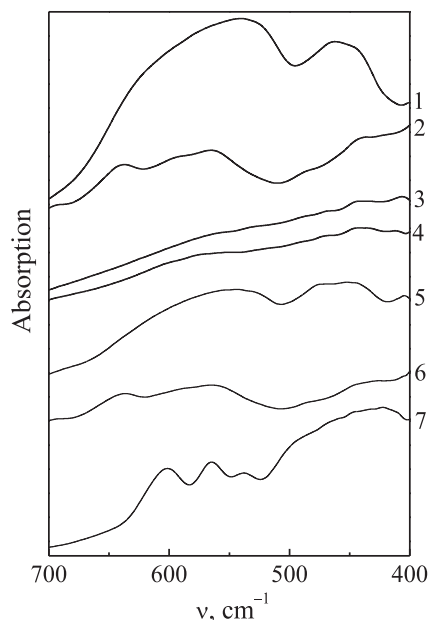


Fig. 2. The characteristic range of the IR spectra of the $\text{Fe}_2\text{O}_3\text{-In}_2\text{O}_3$ (9:1) composites and pure oxides annealed at $400\text{ }^\circ\text{C}$: 1 – sample 5; 2 – sample 7; 3 – sample 3; 4 – sample 11; 5 – $\alpha\text{-Fe}_2\text{O}_3$; 6 – $\gamma\text{-Fe}_2\text{O}_3$; 7 – In_2O_3 .

3.2. Gas-sensing properties

All the studied $\text{Fe}_2\text{O}_3\text{-In}_2\text{O}_3$ thin-film sensors demonstrate lack of sensitivity to CH_4 and CO . This makes them promising candidates for the development of sensors selective to other gases, in particular, to $\text{C}_2\text{H}_5\text{OH}$, NO_2 and O_3 .

3.2.1. Sensitivity to oxidizing gases

The studied $\gamma\text{-Fe}_2\text{O}_3\text{-In}_2\text{O}_3$ films (samples 7–10) demonstrate a high sensitivity to O_3 and NO_2 at low operating temperatures. Their maximum responses to these gases lay in the range of $70\text{--}135\text{ }^\circ\text{C}$, whereas all the mentioned sensors have negligible signals at $250\text{--}300\text{ }^\circ\text{C}$. Samples 1, 3 and 11 based on $\alpha\text{-Fe}_2\text{O}_3$ oxide display low response to the oxidizing gases.

The maximum response values and the optimal operating temperatures to detect NO_2 ambient with In_2O_3 and $\text{Fe}_2\text{O}_3\text{-In}_2\text{O}_3$ sensors are compared together in Table 2. From the reported data it is seen that sample 5, which differ from the other $\gamma\text{-Fe}_2\text{O}_3$ based composites in structural composition, is the most sensitive to NO_2 gas.

Among the studied composite materials, one can mark out two sensors (samples 5 and 9) whose sensitivity to O_3 and NO_2 are

Table 2
The phase composition and the gas-sensing features of the samples to NO_2 (0.5 ppm).

Sample No	Phase composition	T , $^\circ\text{C}$	S , r.u.
In_2O_3 [22]	$\text{C-In}_2\text{O}_3$	100	30
		135	35
5	$\text{Q-}\gamma\text{-Fe}_2\text{O}_3$, $\text{C-}\gamma\text{-Fe}_2\text{O}_3$, $\alpha\text{-Fe}_{2-x}\text{In}_x\text{O}_3$	70	50
		100	75
9	$\text{C-}\gamma\text{-Fe}_2\text{O}_3$, $\text{C-In}_2\text{O}_3$	70	10
		100	20
7	$\text{C-}\gamma\text{-Fe}_2\text{O}_3$, $\text{C-In}_2\text{O}_3$	135	65
8	$\text{C-In}_2\text{O}_3$, $\text{C-}\gamma\text{-Fe}_2\text{O}_3$	100	30
		70	20
10	$\text{C-In}_2\text{O}_3$, $\text{C-}\gamma\text{-Fe}_2\text{O}_3$	100	50
1	$\alpha\text{-Fe}_2\text{O}_3$, $\text{C-In}_2\text{O}_3$	135	1

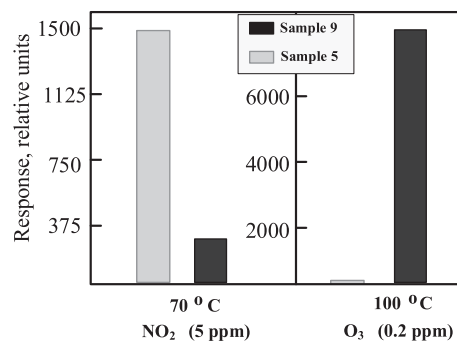


Fig. 3. The response of the $\text{Fe}_2\text{O}_3\text{-In}_2\text{O}_3$ (9:1) sensors to NO_2 and O_3 as a function of the composite microstructure at different operating temperatures.

considerably distinct in different temperature ranges as visually demonstrated by a diagram in Fig. 3.

The response values are given at concentrations higher than the threshold levels. At $70\text{--}100\text{ }^\circ\text{C}$, sample 5 shows a sensitivity maximum to NO_2 and no response to O_3 . Its sensitivity maximum to O_3 is shifted to $150\text{ }^\circ\text{C}$ when the signal to NO_2 is low. In contrast, sample 9 is highly sensitive to O_3 and non-sensitive NO_2 at $100\text{ }^\circ\text{C}$. The indicated variety in the behavior of composites 5 and 9 are evidently caused by the distinctions in their phase composition and grain size (Table 1).

The sensing features of thin-film materials to a certain gas are hardly predictable. Specifically, the sensitivity of thin-film oxide sensors to O_3 and NO_2 is known to depend on many variables like chemical composition, crystalline structure and grain size of sensing layers [1,15,24,44,45]. Both nanosized state and highly defective structure of metal oxides prepared by sol-gel approach cause their enhanced response to oxidizing gases such as O_3 and NO_2 . Based on the data obtained in this study and available from literature, one can suggest a possible reason for the sensing behavior of samples 5 and 9 described above. Their unequal sensitivity to the oxidizing gases might be explained both by distinctions in the microstructure of the $\text{Fe}_2\text{O}_3\text{-In}_2\text{O}_3$ composites and by unequal adsorption affinity of NO_2 and O_3 molecules to porous metal oxides [45,46].

The sensitivity to NO_2 and O_3 depends on the balance of the adsorption and reaction ability of an oxide surface [44–48]. Composite materials containing both effective adsorption centers, and highly conductive microcrystals and grain boundaries provide an enhanced sensor sensitivity.

The adsorption mechanism of the electrical conductivity change

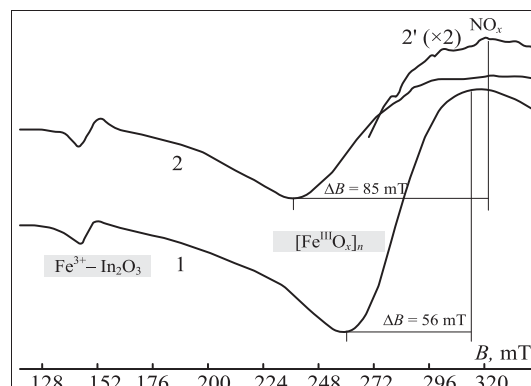


Fig. 4. The EPR spectra of sample 5: 1 – initial; 2 – after exposure to NO_2 -air mixture at $120\text{ }^\circ\text{C}$.

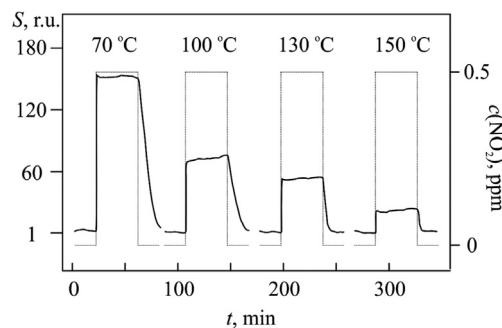


Fig. 5. The dynamic response curves of sensor 5 to 0.5 ppm of NO₂ recorded at different working temperatures.

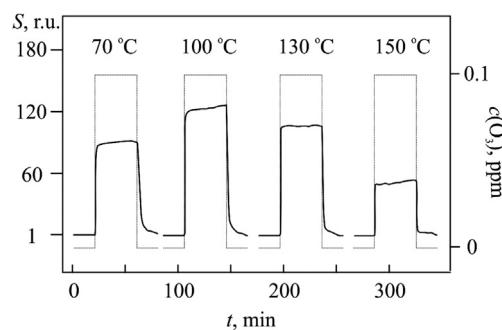


Fig. 6. The dynamic response curves of sensor 9 to 0.1 ppm of O₃ recorded at different working temperatures.

was shown earlier to be dominating for metal oxides (in particular, In₂O₃) when exposed to NO₂ acceptor-type molecules at 100–150 °C [44,45]. Below 150 °C, NO₂ gas remains in a molecular (not reduced) form, which was confirmed by the EPR characterization of the samples studied here (Fig. 4). Thus, a weak triplet signal typical of NO₂ radicals (average *g*-factor is 2.003) is registered in the spectrum of sample 5 after its exposure to NO₂ at 120 °C (spectrum 2). The signal is unambiguously attributed to NO₂ species due to the hyperfine splitting with a constant *A* = 5.9 mT (spectrum 2') arisen from ¹⁴N nuclei (nuclear spin is 1). However, the desorption of NO₂ molecules from the oxide surface proceeds slowly at low temperatures, which could result in a slow dynamics of sensors. Two intensive lines found in both EPR spectra are attributed to Fe³⁺–In₂O₃ solid solution and [Fe^{III}O_x]_n oxide state.

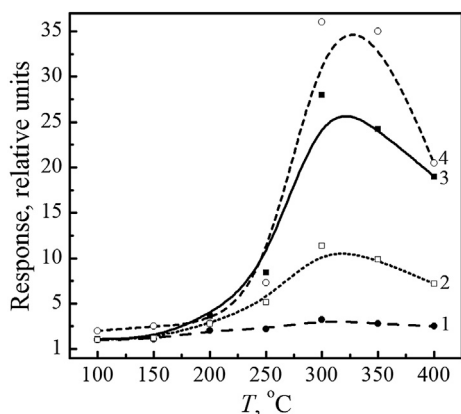


Fig. 7. The temperature-dependent response to 50 ppm of C₂H₅OH of the Fe₂O₃–In₂O₃ layers: 1 – sample 1; 2 – sample 11; 3 – sample 5; 4 – sample 7.

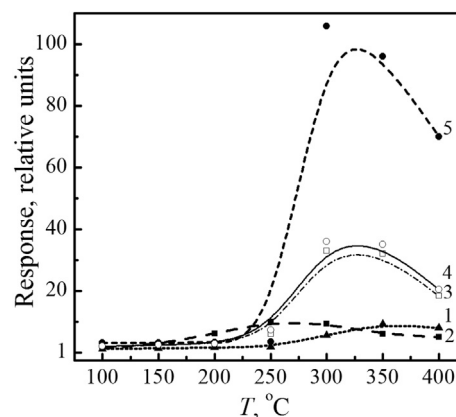


Fig. 8. The temperature-dependent response to 50 ppm of C₂H₅OH of the single oxide and Fe₂O₃–In₂O₃ layers: 1 – In₂O₃; 2 – γ-Fe₂O₃; 3 – bi-layer γ-Fe₂O₃/In₂O₃; 4 – sample 7; 5 – sample 8.

Molecules of NO₂ can get deep inside highly porous materials [46]. Their decomposition proceeds at the whole oxide surface including inner pores. A meso- and macro-porous structure required for an effective adsorption of NO₂ molecules is likely typical of sample 5 consisting of grains, which differ substantially in phase composition, grain size and morphology. The obtained results correlate with the literature data reported a high sensitivity to NO₂ of oxide materials modified with meso- and macro-porous SnO₂ and In₂O₃ oxides [49–51]. However, the desorption of NO₂ molecules and the products of their transformation is slow at low temperatures [45], which causes a long relaxation time of sensors. As it is seen from Fig. 5, the response and recovery times *t*_{resp}/*t*_{rec} are 55/850 s for the detection of 0.5 ppm of NO₂ at 70 °C (sample 5). The relaxation times could be greatly reduced by applying increased working temperatures (130–150 °C), at which the response values of the Fe₂O₃–In₂O₃ sensors to NO₂ are still high. The *t*_{resp}/*t*_{rec} times measured at 130 and 150 °C are 30/220 s and 25/200 s, respectively.

In contrast to NO₂, the detection of O₃ proceeds through the adsorption of oxygen atoms instead of ozone molecules whose decomposition (O₃ → O₂ + O) occurs in a gas phase at 70 °C. This prevents the adsorption of O₃ molecules and their heterogeneous decomposition at an oxide surface [47]. Due to a high chemical reactivity, the generated oxygen atoms are unable to pass inside a porous oxide structure [46]. A low-temperature mode of O₃ detection (100–170 °C) is typical of sensors based on In₂O₃ and γ-Fe₂O₃ due to acceptable dynamic parameters [1,24,44,45]. The *t*_{res}/*t*_{rec} times measured for sample 9 are 40/200 s when detecting 0.1 ppm of O₃ at 100 °C (Fig. 6). The less sensitive samples demonstrate significantly slower values (*t*_{res} = 40 ÷ 100 s,

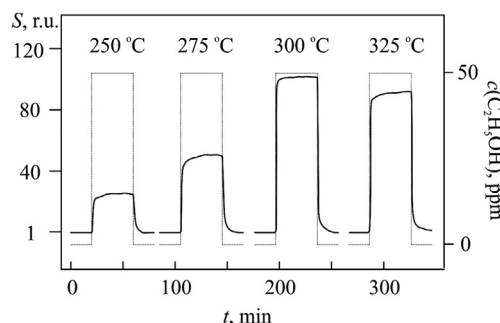


Fig. 9. The dynamic response curves of sensor 8 to 50 ppm of ethanol recorded at different working temperatures.

Table 3

The optimal compositions of the samples and the operating conditions to detect different gases.

Gas	C_{\min} , ppm	T , °C	S , r.u.	Fe:In mol. ratio	Major phase	Minor phase	Sample No
O ₃	0.1	100	130	9:1	C- γ -Fe ₂ O ₃	C-In ₂ O ₃	9
NO ₂	0.5	100	75	9:1	Q- γ -Fe ₂ O ₃	C- γ -Fe ₂ O ₃ , α -Fe _{2-x} In _x O ₃	5
C ₂ H ₅ OH	50	300	105	1:1	C-In ₂ O ₃	C- γ -Fe ₂ O ₃	8

$$t_{\text{rec}} = 1400 \div 1800 \text{ s}).$$

The crystalline structure of oxides appear to be a predominating factor for O₃ detection processes. An effective detection of O₃ is known to proceed on sensing layers based on metastable γ -Fe₂O₃ oxide. Their advanced sensitivity to O₃ is related to a high adsorption ability of spinel-type γ -Fe₂O₃, a fast adsorption-desorption of O₂ [44,45], and an easiness and reversibility of Fe³⁺ + e⁻ ↔ Fe²⁺ transition [24]. C- γ -Fe₂O₃ phase predominates over C-In₂O₃ in sample 9, which causes its increased selectivity to O₃. Note that thin film layers based on C-In₂O₃ also have a high sensitivity to O₃ and NO₂ at 100–150 °C [44,51]; however, they are characterized by lack of selectivity.

3.2.2. Sensitivity to ethanol

All studied Fe₂O₃–In₂O₃ composites are sensitive to C₂H₅OH vapors (50 ppm) at 250–350 °C with a maximum response at 300 °C. As it was noted above, no response to O₃ and NO₂ is typical of the sensors in this temperature range. However, the response to ethanol varies for different samples as a function of their composition and microstructure. As it follows from Figs. 7 and 8, the composites with an equal C- γ -Fe₂O₃ and C-In₂O₃ content are the most sensitive to ethanol vapors.

The mechanism of ethanol detection with complex metaloxide layers, in particular, with Fe₂O₃–In₂O₃ materials, is discussed in [2,48,52]. It is considered as a multi-stage process including the stages of reduction–oxidation and acid–base interactions of ethanol molecules on an oxide surface. The detection of deuterium marked ethanol (C₂H₅OD) with SnO₂ sensors allowed revealing a variety of products generated as a result of the decomposition of this molecule [48].

The materials containing several centers of adsorption and catalysis with close characteristics are the most sensitive to ethanol [53,54]. The Fe₂O₃–In₂O₃ nanocomposites prepared in this paper meet the mentioned requirement. A C-In₂O₃/C- γ -Fe₂O₃ phase interface plays a role of an active surface at which the transformation of ethanol proceeds effectively. The occurrence of two type centers of different nature in our composites provides a multi-way pass of ethanol molecule decomposition and complete oxidation of intermediates. A partial reduction of metal ions without changes in the phase composition is possible for some metal oxides. These oxides are effective promoters of an oxidative dehydration of alcohols [2,53,54]. In particular, easily reversible In³⁺ ↔ In²⁺ and Fe³⁺ ↔ Fe²⁺ equilibriums, which are not accompanying with any phase transitions, are typical of C-In₂O₃ and C- γ -Fe₂O₃ oxides. The low energy of metal-oxygen bonds in the mentioned oxides promotes an oxidation of the intermediate products in the reaction of ethanol decomposition [54], which leads to the growth of sensor responses. The described type of sensing layers is characterized by acceptable dynamics at 300 °C, which is optimal temperature for ethanol detection. The parameters $t_{\text{res}}/t_{\text{rec}} = 40/55$ for sample 8 were found from Fig. 9 in case of 50 ppm of ethanol at 300 °C.

Basing on the obtained results, Fe₂O₃–In₂O₃ materials suitable to produce thin-film sensors potentially selective to O₃, NO₂ and C₂H₅OH are proposed. The corresponding optimal chemical and phase composition of the layers, and the detection conditions are

given in Table 3.

Note, that the given regularities are valid for the sol–gel derived Fe₂O₃–In₂O₃ materials with the reported component ratio, phase composition and morphology, and obtained in a form of thin films [31]. Any modifications in the synthesis conditions might result in materials with different properties. The gas-sensing behavior of In₂O₃ and Fe₂O₃ oxides depends on a variety of structural parameters, which are dependent on the preparation conditions. There is literature reporting unequal sensing properties of In₂O₃ oxide prepared in form of films, porous layers, spherical nanoparticles, nanocubes, hollow spheres, nanorods, nanowires, nanotubes, flowers, nanotowers [5].

4. Conclusions

The sol–gel approach based on inorganic metal precursors was used to obtain Fe₂O₃–In₂O₃ (9:1, 1:1) nanocomposites with different microstructure and grain size. The grain size, the chemical and phase composition of the samples were correlated with their gas-sensing parameters. Hetero-junction Fe₂O₃–In₂O₃ nanocomposites based on cubic C-In₂O₃ phase, which is active in adsorption of gases, were prepared. The synthesis conditions that result in the formation of metastable cubic C- γ -Fe₂O₃ phase in the Fe₂O₃–In₂O₃ composites were revealed. This phase stabilized in the Fe₂O₃–In₂O₃ thin films was found to be more active in adsorption and catalytic transformations of O₃, NO₂ and C₂H₅OH vapors as compared to thermodynamically stable α -Fe₂O₃ phase. The possibility to stabilize a nanosized In-doped Q- γ -Fe₂O₃ phase with an improved sensitivity to NO₂ was shown. The described variety of structural features of the obtained materials provides the possibility to select oxide composites preferable to detect a required gas ambient. The optimal chemical and structural compositions of the Fe₂O₃–In₂O₃ thin-film sensing layers and operating temperatures were proposed to detect a series of gases – O₃, NO₂ and C₂H₅OH. It was shown that the optimal working temperatures of the proposed sensors are significantly lower than the temperatures inducing phase transformations in the Fe₂O₃–In₂O₃ composites. This provides the long-term stability of their sensing parameters. Note that an optimization of the functional features of the developed materials is still required for their commercial use. In particular, the dynamic parameters and the influence of humidity on the response of the sensors should be considered. For example, some techniques that allow minimizing the humidity effect on the signal are commonly used in commercially available sensors. Satisfactory dynamic parameters of the sensors could be achieved by applying different heating modes of the sensing elements like higher working temperatures and a pulse mode of heating.

References

- [1] M. Ivanovskaya, D. Kotsikau, G. Faglia, P. Nelli, S. Irkaev, Gas-sensitive properties of thin film heterostructures based on Fe₂O₃–In₂O₃ nanocomposites, Sens. Actuators B 93 (2003) 422–430, <http://dx.doi.org/10.1016/j.snb.2004.02.051>.
- [2] M. Ivanovskaya, D. Kotsikau, G. Faglia, P. Nelli, Influence of chemical composition and structural factors of Fe₂O₃/In₂O₃ sensors on their selectivity and sensitivity to ethanol, Sens. Actuators B 96 (2003) 498–503, [http://dx.doi.org/10.1016/S0925-4005\(03\)00624-5](http://dx.doi.org/10.1016/S0925-4005(03)00624-5).
- [3] T. Zhou, L. Wei, Y. Xie, Q. Li, G. Hu, Y. Chen, Effects of Sn doping on the

- morphology and properties of Fe-doped In_2O_3 epitaxial films, *Nanoscale Res. Lett.* 7 (2012) 1–7, <http://dx.doi.org/10.1186/1556-276X-7-661>.
- [4] G. Han, Q. Lu, G. Liu, X. Ye, S. Lin, Y. Song, G. Li, Enhanced ethanol sensing properties based on $\alpha\text{-Fe}_2\text{O}_3/\text{In}_2\text{O}_3$ hollow microspheres, *J. Mater. Sci. Mater. Electron.* 23 (2012) 1616–1620, <http://dx.doi.org/10.1007/s10854-012-0638-4>.
- [5] P. Li, Y. Cai, H. Fan, Porous thin sheet-based $\alpha\text{-Fe}_2\text{O}_3$ -doped In_2O_3 structures: hydrothermal synthesis and enhanced Cl_2 sensing performance, *RSC Adv.* 3 (2013) 22239–22245, <http://dx.doi.org/10.1039/C3RA43616K>.
- [6] R.K. Gupta, K. Ghosh, P.K. Kahol, Room temperature ferromagnetic multilayer thin film based on indium oxide and iron oxide for transparent spintronic applications, *Mater. Lett.* 64 (2010) 2022–2024, <http://dx.doi.org/10.1016/j.matlet.2010.06.026>.
- [7] D. Berardan, E. Guilmeau, Magnetic properties of bulk Fe-doped indium oxide, *J. Phys. Condens. Matter.* 19 (2007) 236224, <http://dx.doi.org/10.1088/0953-8984/19/23/236224>, 9.
- [8] A. Singhal, S.N. Achary, J. Manjanna, O.D. Jayakumar, R.M. Kadam, A.K. Tyagi, Colloidal Fe-doped indium oxide nanoparticles: facile synthesis, structural and magnetic properties, *J. Phys. Chem. C* 113 (2009) 3600–3606, <http://dx.doi.org/10.1021/jp8097846>.
- [9] S. Kohiki, Y. Murakawa, K. Hori, H. Shimooka, T. Tajiri, H. Deguchi, M. Oku, M. Arai, M. Mitome, Y. Bando, Magnetic behavior of Fe-doped In_2O_3 , *Jpn. J. Appl. Phys.* 44 (2005) L979–L981, <http://dx.doi.org/10.1143/JJAP.44.L979>.
- [10] S.B. Qadri, C. Fahed, N.A. Mahadik, H. Kim, M. Osofsky, M.V. Rao, Deposition of $\text{In}_2\text{-xFe}_x\text{O}_3$ films by ultrafast microwave heating technique, *J. Mater. Sci. Eng. A* 1 (2011) 869–871.
- [11] C. Fahed, S.B. Qadri, H. Kim, A. Piqué, M. Miller, N.A. Mahadik, M.V. Rao, M. Osofsky, Transport, magnetic and structural properties of bulk $\text{In}_{2-x}\text{Fe}_x\text{O}_3$, *Phys. Status Solidi C* 7 (2010) 2298–2301, <http://dx.doi.org/10.1002/pssc.200983703>.
- [12] M. Ristic, S. Popovich, M. Tonkovich, Chemical and structural properties of the system $\text{Fe}_2\text{O}_3\text{-In}_2\text{O}_3$, *J. Mater. Sci.* 26 (1991) 4225–4233, <http://dx.doi.org/10.1007/BF02402973>.
- [13] G. Han, Q. Lu, G. Liu, X. Ye, S. Lin, Y. Song, B. Liu, X. Yang, G. Li, Enhanced ethanol sensing properties based on $\alpha\text{-Fe}_2\text{O}_3/\text{In}_2\text{O}_3$ hollow microspheres, *J. Mater. Sci. Mater. Electron.* 23 (2012) 1616–1620, <http://dx.doi.org/10.1007/s10854-012-0638-4>.
- [14] M. Sorescu, T. Xu, L. Diamandescu, D. Hileman, Synthesis and characterization of indium oxide-hematite magnetic ceramic solid solution, *Hyperfine Interact.* 199 (2011) 365–386, <http://dx.doi.org/10.1007/s10751-011-0267-y>.
- [15] M. Ivanovskaya, D. Kotsikau, A. Taurino, P. Siciliano, Structural distinctions of $\text{Fe}_2\text{O}_3\text{-In}_2\text{O}_3$ composites obtained by various sol-gel procedures, and their gas-sensing features, *Sens. Actuators B* 124 (2007) 133–142, <http://dx.doi.org/10.1016/j.snb.2006.12.011>.
- [16] Z. Jing, Synthesis, characterization and gas sensing properties of undoped and Zn-doped $\gamma\text{-Fe}_2\text{O}_3$ -based gas sensors, *Mat. Sci. Eng. A* 441 (2006) 176–180, <http://dx.doi.org/10.1016/j.msea.2006.08.013>.
- [17] J.M. Tulliani, P. Bonville, Influence of the dopants on the electrical resistance of hematite-based humidity sensors, *Ceram. Int.* 31 (2005) 507–514, <http://dx.doi.org/10.1016/j.ceramint.2004.06.015>.
- [18] G. Neri, A. Bonavita, S. Galvagno, N. Donato, A. Caddemi, Electrical characterization of Fe_2O_3 humidity sensors doped with Li^+ , Zn^{2+} and Au^{3+} ions, *Sens. Actuators B* 111–112 (2005) 71–77, <http://dx.doi.org/10.1016/j.snb.2005.06.061>.
- [19] I. Nodari, A. Alebouyeh, J.F. Brice, R. Gerardin, O. Evrard, Caractérisation de nouveaux ferrites d'indium: $\text{In}_2\text{Fe}_4\text{O}_9$ et InFeO_3 , *Mater. Res. Bull.* 23 (1988) 1039–1044, [http://dx.doi.org/10.1016/0025-5408\(88\)90060-8](http://dx.doi.org/10.1016/0025-5408(88)90060-8).
- [20] F. Brown, M. Flores, N. Kimuzuka, Y. Michiue, M. Onoda, T. Mohri, M. Nakamura, N. Ishizawa, Phase relation in system $\text{In}_2\text{O}_3\text{-TiO}_2\text{-Fe}_2\text{O}_3$ at 1100°C in air, *J. Solid State Chem.* 144 (1999) 91–99, <http://dx.doi.org/10.1006/jssc.1998.8123>.
- [21] M. Pernet, J.C. Joubert, Etude par diffraction neutronique de la forme haute pression de FeOOH , *Solid State Comm.* 17 (1975) 1505, [http://dx.doi.org/10.1016/0038-1098\(75\)90983-7](http://dx.doi.org/10.1016/0038-1098(75)90983-7).
- [22] A. Gurlo, M. Ivanovskaya, N. Barsan, U. Weimar, Corundum-type indium (III) oxide: formation under ambient conditions in $\text{Fe}_2\text{O}_3\text{-In}_2\text{O}_3$ system, *Inorg. Chem. Commun.* 6 (2003) 569–572, [http://dx.doi.org/10.1016/S1387-7003\(03\)00047-9](http://dx.doi.org/10.1016/S1387-7003(03)00047-9).
- [23] J. Shin, S. Park, Some characteristics of $\gamma\text{-Fe}_2\text{O}_3$ ceramic gas sensors, in: *Proc. Of the 2nd Int. Meeting on Chemical Sensors, Bordeaux, 1986*, pp. 123–126.
- [24] E. Gutman, Ozone sensor for the earth ozonosphere investigations, *Sens. Actuators B* 25 (1996) 135–146, [http://dx.doi.org/10.1016/0925-4005\(94\)01276-N](http://dx.doi.org/10.1016/0925-4005(94)01276-N).
- [25] U. Schwertmann, R.M. Cornell, Iron Oxides in the Laboratory: Preparation and Characterization, VCH Verlagsgesellschaft mbH, Weinheim, 1991, [http://dx.doi.org/10.1016/0010-938X\(92\)90174-2](http://dx.doi.org/10.1016/0010-938X(92)90174-2).
- [26] J.L. Jambor, J.E. Dutrizac, Occurrence and constitution of natural and synthetic ferrihydrite, a widespread iron oxyhydroxide, *Chem. Rev.* 98 (1998) 2549–2585, <http://dx.doi.org/10.1021/cr970105t>.
- [27] L.E. Smart, E.A. Moore, *Solid State Chemistry*, Chapman & Hall, London, 1995.
- [28] C.J. Brinker, G.W. Scherer, *Sol-gel Science: The Physics and Chemistry of Sol-gel Processing*, 1990, AP, London.
- [29] J. Livage, M. Henry, C. Sanchez, Sol-gel Chemistry of transition metal oxides, *Prog. Solid State Chem.* 18 (1988) 259–341, [http://dx.doi.org/10.1016/0079-6786\(88\)90005-2](http://dx.doi.org/10.1016/0079-6786(88)90005-2).
- [30] E.V. Frolova, M.I. Ivanovskaya, Structural defects formation in the inorganic sol-gel derived oxides, *Defect Diffusion Forum* 242–244 (2005) 143–258.
- [31] M. Ivanovskaya, Ceramic and film metaloxide sensors obtained by sol-gel method: structural features and gas-sensitive properties, *Electron Technol.* 33 (2000) 108–112.
- [32] C.M. Flynn, Hydrolysis of inorganic iron(III) salts, *Chem. Rev.* 84 (1984) 31–41.
- [33] R.M. Cornell, R. Giovanoli, W. Schneider, Review of the hydrolysis of iron (III) and the crystallization of amorphous iron(III) hydroxide hydrate, *J. Chem. Technol. Biotechnol.* 46 (1989) 115–134.
- [34] L. Vayssier, C. Chaneac, E. Tronc, J.P. Jolivet, Size tailoring of magnetite particles by aqueous precipitation: an example of thermodynamic stability of nanometric oxide particles, *J. Colloid. Int. Sci.* 205 (1998) 205–212, <http://dx.doi.org/10.1006/jcis.1998.5614>.
- [35] Y.S. Kang, S. Risbud, J.F. Rabolt, P. Stroev, Synthesis and characterization of nanometer size Fe_3O_4 and $\gamma\text{-Fe}_2\text{O}_3$ particles, *Chem. Mater.* 8 (1996) 2209–2211.
- [36] S. Sun, H. Zeng, Size-controlled synthesis of magnetite nanoparticles, *J. Am. Chem. Soc.* 124 (2004) 8204–8205, <http://dx.doi.org/10.1021/ja026501x>.
- [37] M. Macias, J. Morales, J.C. Tirado, C. Valera, Effect of crystallinity on the thermal evolution of $\gamma\text{-Fe}_2\text{O}_3$, *Thermochim. Acta* 133 (1998) 107–112.
- [38] A.A. Davydov, *Molecular Spectroscopy of Oxide Catalyst Surfaces*, Wiley, New York, 2003.
- [39] G. Ennas, G. Marongui, A. Musinu, A. Falqui, P. Ballirano, R. Caminity, Characterization of nanocrystalline $\gamma\text{-Fe}_2\text{O}_3$ prepared by wet chemical method, *J. Mater. Res.* 14 (1999) 1570–1575.
- [40] C. Greaves, A powder neutron diffraction investigation of vacancy ordering and covalence in $\gamma\text{-Fe}_2\text{O}_3$, *J. Solid State Chem.* 49 (1983) 325–333.
- [41] T. Belin, N. Guigue-Millot, T. Caillot, D. Aymes, J.C. Niepce, Influence of grain size, oxygen stoichiometry, and synthesis conditions on the $\gamma\text{-Fe}_2\text{O}_3$ vacancies Fe_2O_3 and lattice parameters, *J. Solid State Chem.* 163 (2002) 459–465, <http://dx.doi.org/10.1006/jssc.2001.9426>.
- [42] D. Kotsikau, M. Ivanovskaya, D. Orlik, M. Falasconi, Gas-sensitive properties of thin and thick film sensors based on $\text{Fe}_2\text{O}_3\text{-SnO}_2$ nanocomposites, *Sens. Actuators B* 101 (2004) 199–206, <http://dx.doi.org/10.1016/j.snb.2004.02.051>.
- [43] G.N. Kryukova, A.L. Chuvilin, V.A. Sadykov, On the $\gamma\text{-Fe}_2\text{O}_3$ superstructure observation by high resolution electron microscopy, *J. Solid State Chem.* 89 (1990) 208–214, [http://dx.doi.org/10.1016/0022-4596\(90\)90313-M](http://dx.doi.org/10.1016/0022-4596(90)90313-M).
- [44] A. Gurlo, N. Barsan, M. Ivanovskaya, U. Weimar, W. Göpel, In_2O_3 and $\text{In}_2\text{O}_3\text{-MoO}_3$ thin film semiconductor sensors: interaction with NO_2 and O_3 , *Sens. Actuators B* 47 (1998) 92–99, [http://dx.doi.org/10.1016/S0925-4005\(98\)00033-1](http://dx.doi.org/10.1016/S0925-4005(98)00033-1).
- [45] M. Ivanovskaya, A. Gurlo, P. Bogdanov, Mechanism of O_3 and NO_2 detection and selectivity of In_2O_3 sensors, *Sens. Actuators B* 70 (2001) 264–267, [http://dx.doi.org/10.1016/S0925-4005\(01\)00708-0](http://dx.doi.org/10.1016/S0925-4005(01)00708-0).
- [46] V. Ya. Sukharev, I.A. Myasnikov, Theoretical base of semiconducting sensors in analysis of active gases. Influence of adsorption of gases on electrical conductivity of polycrystalline sorbents, *Russ. J. Phys. Chem.* 61 (1987) 302–312.
- [47] V.V. Lunin, M.P. Popovich, S.N. Tkachenko, *The Physical Chemistry of Ozone*, Moscow State University, Moscow, 1998.
- [48] D. Kohl, Surface processes in the detection of reducing gases with SnO_2 -based devices, *Sens. Actuators B* 18 (1989) 71–113, [http://dx.doi.org/10.1016/0250-6874\(89\)87026-X](http://dx.doi.org/10.1016/0250-6874(89)87026-X).
- [49] T. Wagner, T. Sauerwald, C.-D. Kohl, T. Waitz, C. Weidmann, M. Tiemann, Gas sensors based on ordered mesoporous In_2O_3 , *Thin Solid Films* 517 (2009) 6170–6175, <http://dx.doi.org/10.1016/j.tsf.2009.04.013>.
- [50] C. Ishibashi, T. Hyodo, Y. Shimizu, M. Egashira, H_2S sensing properties of macroporous In_2O_3 -based sensors, *Sensors Lett.* 9 (2011) 369–373.
- [51] T. Hyodo, Y. Mitsuyasu, Y. Shimizu, M. Egashira, H_2 and NO_x sensing properties of ZnO and In_2O_3 powders modified with mesoporous SnO_2 , *J. Ceram. Soc. Jpn.* 112 (2004) S540–S545.
- [52] M. Ivanovskaya, P. Bogdanov, G. Flagla, P. Nelli, G. Sberveglieri, On the role of catalytic additives in gas-sensitivity of SnO_2 -based thin film sensors, *Sens. Actuators B* 70 (2001) 268–274, [http://dx.doi.org/10.1016/S0925-4005\(01\)00709-2](http://dx.doi.org/10.1016/S0925-4005(01)00709-2).
- [53] O.V. Krylov, *The Catalysis by Non-metals. The Appropriateness of the Catalysts Selection*, Khimia, Leningrad, 1967.
- [54] G.I. Golodets, Reductive-oxidative and acid-base steps of heterogeneous catalytic oxidizing reaction, in: *Catalysis Mechanism, Part 1*, Nauka, Novosibirsk, 1984, pp. 142–158.